Mini Review
doi.org/10.1002/elsa.202100079

Chemistry Europe
European Chemical Societies Publishing

Received: 5 May 2021
Revised: 19 June 2021
Accepted: 22 June 2021

Metal oxides as electrocatalysts for water splitting: On plasmon-driven enhanced activity

Maria P. de Souza Rodrigues[#] | **Vítor M. Miguel**[#] | **Lucas D. Germano**[#] | **Susana I. Córdoba de Torresi**

Departamento de Química Fundamental, Instituto de Química, Universidade de São Paulo, São Paulo, Brazil

Correspondence
Susana I. Córdoba de Torresi, Departamento de Química Fundamental, Instituto de Química, Universidade de São Paulo, Av. Prof. Lineu Prestes, 748, 05508-000, São Paulo, SP, Brazil.
Email: storresi@iq.usp.br

[#]Equal contributions.

Funding information
Fundação de Amparo à Pesquisa do Estado de São Paulo, Grant/Award Numbers: #2015-26308-7, #2018-16846-0, #2018-22845-6, #2019-15885-4

Abstract

Many technological approaches have been searched in order to overcome the main challenges concerning the world energy crisis and global environmental issues. Among them, plasmon-driven photoelectrochemical reactions towards water electrolysis attract great attention due to their capacity to efficiently harvest solar energy. Synergism between tunable optical features and catalysts active sites of plasmonic nanomaterials gives rise to a singular perspective for photochemical processes. Through resonant photonic excitation, hot carriers' motion facilitates the charge transfer process on the catalyst surface for chemical reactions. In this minireview, recent experimental research with emphasis on water splitting reactions have been summarized with the purpose of understanding the mechanistic hot electrons generation and transfer on the plasmonic noble metal nanoparticles (MNPs) and transition metal oxides (MOs) heterostructures. Examples of plasmonic nanomaterials are highlighted and compared for both water electrolysis semi reactions. Finally, this work concludes by describing the remaining challenges and gives some perspectives regarding the promising future of plasmon-driven reactions investigations.

KEYWORDS
noble metal, oxides, plasmonics, semiconductor, water splitting

1 | INTRODUCTION

In the field of energy, the implementation of new technologies is sought to optimize and develop alternative approaches for electric energy generation. Until now, the world's energetic matrix is based on the consumption of fossil fuels, which can increase global climatic issues[1]. Solar-driven water splitting is a regenerative and greener alternative process that addresses the main heat-driven energy generation drawbacks[2]. In the core of this energy conversion technology, water electrolysis consists of two pairs of reversible electrochemical reactions: oxygen reduction reaction (ORR), hydrogen oxidation reaction (HOR), and oxygen evolution reaction (OER), hydrogen evolution reaction (HER)[3,4]. The electrochemical reactions involving H_2 generation/consumption present relatively faster electron transfer kinetics, when compared to their counterpart reactions. However, the implementation of "hydrogen economy" (hydrogen as fuel for generation of electrical energy on industrial scale) faces

Mini Review
doi.org/10.1002/elsa.202100079
Chemistry Europe
European Chemical Societies Publishing

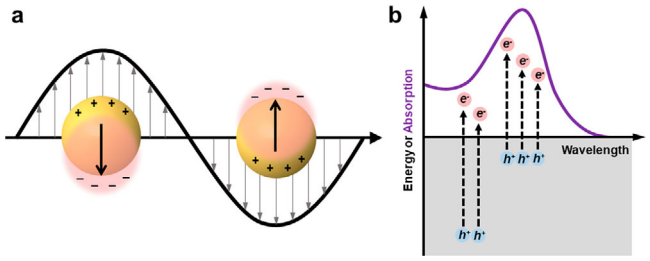

FIGURE 1 **(A)** The LSPR effect on metallic nanoparticles, in which the valence electron coherent oscillation generates a local enhanced electromagnetic field. **(B)** The relation between absorption spectrum, represented in purple line, and the hot electrons and holes (hot carriers), described as e^- and h^+, respectively. Reprinted with permission from ref. [11]. Copyright 2018 American Chemical Society

disadvantages, such as gas storage and the high cost of Pt, which is the benchmark catalyst for HER. However, the reactions involving oxygen species are considered the limiting step of the overall water electrolysis, shortly owing to the requirement of a significant amount of energy and sluggish kinetics caused by the mechanism of multi-electronic transfer[4,5].

Regarding these challenges, metal nanoparticles (MNPs), such as Au, Ag, and Cu, have recently aroused great interest due to the localized surface plasmon resonance (LSPR), generated by the interaction of such metals with light[2,6,7]. When these MNPs are irradiated, the conduction band electrons oscillate due to the electric field of the incident photons. Then, a dipole is formed on the MNPs surface, as the electrons are induced to move in one direction, generating a positive charge in the opposite direction. In specific wavelengths, a resonance is formed by this collective oscillation and gives rise to an enhanced local electromagnetic field and separation of charges due to the generation of hot electrons and holes (Figure 1).[8–10]

The LSPR phenomenon produces hot carriers that can participate in photoelectrochemical reactions. Mechanisms' insights have shown that these carriers can directly interact with adsorbed molecules on MNPs. Plasmonic excited carriers can also be transferred to vicinal semiconductor support materials, by the so-called plasmon-mediated electron transfer (PMET). In this way, hot carrier lifetime can be prolonged, by trapping them in the conduction band of the semiconductor, and avoiding rapid electron-hole recombination on MNPs[11,12]. Moreover, this physical effect is highly dependent on the composition, size, geometry, and spacing of the metallic nanoparticles, making it possible to tune the wavelength required for the LSPR across the visible and near-infrared spectrum[12,13].–

In recent years, plasmon-enhanced techniques have shown very promising advances in areas such as catalysis[14,15], electrochemical sensors[16], biosensing[17], energy storage[18], and water splitting[19]. Concerning energy applications, the possibility of harvesting light on the visible range of the spectrum, in a tunable manner, represents a progress in the fabrication of more efficient materials for the electrochemical production of different kinds of fuels[8,13]. Despite the advantages of LSPR, developing energy devices using noble metals can be expensive, and the hot electron-hole recombination represents a barrier to their efficient application[9,20].

As an alternative for neat noble metal-based materials toward energy applications, transition metal oxides (MOs) have received great attention[21,22]. These oxides present several advantages such as low cost, abundance, easy synthesis, long-term mechanical and chemical stability, and they are clean and environmentally friendly alternatives[23,24]. Nevertheless, MOs application still faces few challenges, as they mostly absorb in the UV region of the spectrum, present high charge recombination rates, and improper band edge position for several reactions. Approaches to address those challenges consist of coupling MOs with dye molecules[25], quantum dots[26], and, more recently, with metallic nanoparticles[27]. When coupled to oxides, MNPs can increase their light harvesting to the visible range of the spectrum, reduce electron-hole recombination, and enhance the MOs catalytic activity[27–29]. For these coupling cases, gold and silver are commonly used for plasmonic applications in the visible range of the spectrum[30]. Ag nanoparticles have stronger plasmon resonance throughout the spectrum (300–1200 nm), with lower rates of intrinsic energy loss[31]. Nonetheless, Au nanoparticles show high stability, oxide-free surface, and biocompatibility and are usually preferred[30,32].

This minireview focuses on the recent progress of plasmon-driven enhancement of the photoelectrochemical reactions toward water splitting, showing the state-of-art nanostructures based on noble metal nanoparticles and transition metal oxides. The discussion ahead describes detailed water splitting processes (Section 2), and then, it is divided into two subsections. The first one, (Section 2.1) dealing with hydrogen evolution reaction (HER), explores recent nanomaterial developments and mechanistic insights of the possible electron-transfer pathway considering the plasmonic effect and the semiconductor electronic structure. Section 2.2 is reserved for the discussion of oxygen evolution reaction (OER), presenting recent developments and mechanistic particularities, as aforementioned for the HER section. By the end (Sections 3 and 4), some conclusions and future perspectives for the challenges currently encountered in the matter of the plasmon-driven photoelectrochemical reactions in oxide semiconductors, are presented.

Mini Review
doi.org/10.1002/elsa.202100079
Chemistry Europe
European Chemical Societies Publishing

2 | WATER SPLITTING

The overall water splitting consists of two half-reactions, the hydrogen and oxygen evolution reaction (HER and OER, respectively), and their equation and equilibrium potential (E_{eq}) can be seen as below[33]:

$$4H^+ + 4e^- \rightarrow 2H_2 E_{eq} = (0 - 0.059pH)\,V_{RHE}$$

$$2H_2O \rightarrow O_2 + 4H^+ + 4e^- E_{eq} = (1.23 - 0.059pH)\,V_{RHE}$$

The HER reaction follows a two-electron transfer to generate hydrogen. The reaction kinetics of HER is faster when compared to the OER, due to the simplicity of its reactants and products and, consequently, lower energy input[5]. In acidic media, the general HER mechanism can be described by two of the three reaction steps: Volmer-Heyrovsky or Volmer-Tafel. The Volmer step is the electrochemical hydrogen adsorption, leading to the formation of the hydrogen intermediate (H^*) on the catalyst surface[34]. After the Volmer step, two paths are possible: the Heyrovsky, which is electrochemical desorption of the intermediate, or the Tafel step, which is its chemical desorption[35]. The HER mechanism depends on the catalyst nature, and an optimal catalyst toward the reaction is considered to have a moderate metal-hydrogen (M-H) bond energy, facilitating the adsorption and desorption process[36,37]. The limiting reaction step is determined by the Tafel slope from the polarization curve of the HER. The equations and Tafel slope of each step can be seen as below:

Volmer Step $H^+ + e^- \rightarrow H^*\,(118.2mV/dec)$

Heyrovsky Step $H^* + H^+ + e^- \rightarrow H_2\,(39.4mV/dec)$

Tafel Step $H^* + H^* \rightarrow H_2\,(29.6\ mV/dec)$

On the other hand, the OER is a more complex reaction and is considered the limiting step of the overall water electrolysis[37]. It consists of a multistep reaction with four consecutive single-electron transfer steps[31]. This reaction presents a sluggish kinetic and requires a significant amount of energy in order to overcome the thermodynamic barrier ($E^0 = 1.23$ V)[4,5]. Although there are several proposed mechanisms for the OER, the most accepted is described as below[24,37]:

$$M + H_2O \rightarrow MOH + H^+ + e^-$$

$$MOH \rightarrow MO + H^+ + e^-$$

$$2MO \rightarrow 2M + O_2 + 2e^-$$

or

$$MO + H_2O \rightarrow MOOH + H^+ + e^-$$

$$MOOH + H_2O \rightarrow M + O_2 + H^+ + e^-$$

As reported for the HER, an intermediate binding energy of the metal and reaction intermediates (as *OH, O*, and HOO*) plays a key role in obtaining an optimal catalyst[37,38], as well as good stability and small overpotentials[31]. To implement such alternative technology, a myriad of distinct materials has been designed and investigated in the past few years, aiming at gathering the benefits from natural abundant resources, such as water and sunlight.

2.1 | Hydrogen evolution reaction

Among MOs materials, zinc oxide (ZnO) has attracted attention in photocatalysis due to its remarkable properties, such as its easy crystallization, high chemical stability, facile synthesis, high electron mobility (200-300 $cm^2\ V^{-1}\ s^{-1}$), and photosensitivity. Nonetheless, its wide bandgap (3.37 eV) and high exciton binding energy (60 meV) are the major drawbacks toward its application in photocatalysis[39,40].

ZnO has been modified with several noble metals such as Ag, Au,[41] and Cu[42]. However, gold presents a higher capability of effectively promoting the charge carrier separation, due to its work function (5.1 eV). The work function indicates the direction in which the electrons will flow, and the electron transfer will only happen when there is a difference in work function[43]. When the NP work function is higher than that of the MO, electrons will flow from NP to MO. However, when the work function of MO is higher, electrons will be transferred from MO to NP[44]. As the gold work function is higher, it guarantees that the electron

Mini Review
doi.org/10.1002/elsa.202100079
Chemistry Europe
European Chemical Societies Publishing

TABLE 1 Comparative materials for HER

Materials	Light source	Electrolyte	Photoconversion	j (mA/cm^2)	Reference
Au/B-ZnO NW	300 W Xe lamp 100 mW/cm^2	0.5 M Na_2SO_4	0.52%@0.8 V_{RHE}	1.45 @ 1.0 V_{RHE}	[46]
Au/ZnO NW	300 W Xe lamp 100 mW/cm^2	0.5 M Na_2SO_4	0.45%@0.8VRHE	1.06 @ 0.8 VRHE	[47]
ZnO NS/Au	Xe lamp 100 mW/cm^2	0.5 M Na_2SO_4	0.51%@0.23 VAg/AgCl	1.26 @ 0.6 VAg/AgCl	[48]
Au/ZnO NR	300 W Xe lamp 100 mW/cm^2	0.1 M Na_2SO_4	-	30×10–3 @ 0.8 VAg/AgCl	[49]
Au-ZnO	150 W Halogen lamp 100 mW/cm^2	0.1 M Na_2SO_4	0.48%@1.0 VRHE	9.11 @ 1.0 VAg/AgCl	[52]
Au-ZnO	Xe lamp 100 mW/cm^2	0.5 M Na_2SO_4	-	20×10–3 @ 0.0 VAg/AgCl	[51]
Au@ZnO	Xe lamp 100 mW/cm^2	0.25 M Na_2S + 0.35 M Na_2SO_3	-	3.0@ 0.4 VAg/AgCl	[111]
Au-ZnO	Xe lamp 100 mW/cm^2	0.5 M Na_2SO_4	-	1.5 @ 1 VAg/AgCl	[112]
3D Au-in-TiO_2	Xe lamp	25% Methanol	-	1.8×10–3 @ 0.2 VAg/AgCl	[68]
Au/TiO_2	200 W Hg (Xe) lamp	0.5 M H_2SO_4 + 50 mM methanol	-	5×10–9 @ OCP	[110]
Au/TiO_2/Au	AM 1.5 G 100 mW/cm^2	1M KOH	-	9×10–3 @ 0 VAg/AgCl	[62]
Au/TiO_2	Visible light source	0.1 M KOH	-	0.1×10–3 @ 0.6 VAg/AgCl	[113]
Au-TiO_2	300 W Xe lamp	0.5 M Na_2SO_4	-	130×10–3	[63]
Au/TiO_2	AM 1.5G 100 mW/cm^2	0.1 M KH_2PO_4 + 25% methanol	-	2×10–3 @ 0.4 VRHE	[64]
Au/TiO_2	AM 1.5 G 100 mW cm^{-2}	0.05 M Na_2SO_4	-	4×10–3@ 0 VAg/AgCl	[65]
TiO_2-on-Au	Xe lamp	0.1 M Na_2SO_4	-	0.12	[114]

transfer process will happen from the oxide to Au, and not in the opposite sense. As Ag work function is lower (4.26 eV) when compared to gold, this metal is less efficient to promote charge carrier separation. Nonetheless, it can still contribute to an improved activity and it has been extensively explored toward the semiconductor improved photocatalytic activity[39,45].

Au/ZnO nanostructures have been explored in various arrangements, including nanowires[46,47], nanosheets[48], nanoarrays[49,50], among others[51] to evaluate their plasmon-enhanced performance toward HER. Table 1 resumes some of the results found in the literature for Au/ZnO plasmon-enhanced HER. For instance, Wu et al.[52] produced a matchlike heterostructure, composed of ZnO nanowire arrays with Au spheres on their tip and evaluated their plasmonic catalytic activity.

The synthesized heterostructure showed a sharp absorption band below 390 nm, which was attributed to ZnO. However, this band was extended until the visible range of the spectrum and centered at 480 nm due to the Au NPs; increasing the ZnO light-harvesting capability. Moreover, photoluminescence and electrochemical impedance spectroscopy (EIS) measurements showed an electron trapping effect when comparing the bare ZnO and the ZnO-Au structures[52]. Bare ZnO showed improved performance with light irradiation; nonetheless, ZnO-Au

Mini Review
doi.org/10.1002/elsa.202100079
Chemistry Europe
European Chemical Societies Publishing

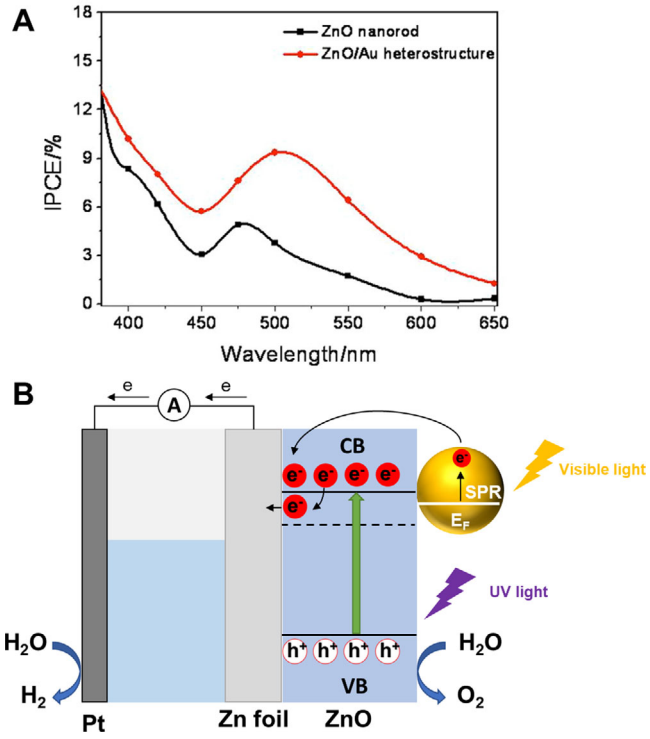

FIGURE 2 **(A)** Incident photon-to-current (IPCE) curves of pristine ZnO nanorod array and matchlike ZnO/Au plasmonic heterostructure photoanode measured from 380 to 600 nm at +0.60 $V_{Ag/AgCl}$ and in 0.1 mol/L Na_2SO_4 and under 100 mW/cm^2 light irradiation (150W xenon lamp with 1.5 AM filter). **(B)** Schematic illustration of the charge separation mechanism under light irradiation for a general ZnO/Au heterostructure. Adapted with permission from ref. [52]. Copyright 2014 American Chemical Society

heterostructure exhibited a 16 times enhancement in efficiency compared to pristine ZnO. The photocurrent observed was 9.11 mA/cm^2 at 1.0 $V_{Ag/AgCl}$, whereas the photoconversion achieved 0.48%. Photon-to-current efficiency (IPCE) measurements showed the activity dependency on the wavelength of the light source (Figure 2A). The highest activity was observed at 500 nm, which is in accordance with the LSPR band in the extinction spectra[52]. The proposed plasmon-enhanced mechanism is described in Figure 2B. When the heterostructure is irradiated by light, ZnO valence band (VB) electrons are photoexcited to its conduction band (CB), generating holes in the VB of the oxide. The excited electrons are transferred from ZnO to gold, decreasing the electron recombination rate due to the electrons' trapping in the nanoparticle. Finally, Au LSPR leads to the production of hot electrons, which are injected in the semiconductor CB. Later, these electrons flow to the Pt counter electrode to produce hydrogen.

Although Ag nanoparticles are less explored than Au due to their lack of stability, some authors have discussed their plasmonic activity combined with ZnO towards HER. When coupled with a support, Ag stability and outstanding plasmonic performance are increased[53]. Several morphologies and arrangements of Ag/ZnO were also explored in the literature[54–57].

Another transition metal oxide that has also been extensively studied toward the water-splitting reaction is titanium dioxide, since its first demonstration by Fujishima and Hond[58]. This oxide attracted much attention due to its low cost, high stability, and superior electronic and chemical properties[59]. However, its application is limited by the high charge recombination rate[60], wide bandgap (3.2 eV), and low solar collection efficiency (4-5% of the total solar spectrum)[61]. Au/TiO_2 nanomaterials have been applied in HER in several studies with different conformations as nanosheets[62], janus[63] and half-dome heterostructures[64], films[65], among others[66,67]. Table 1 resumes some of the results found in the literature for Au/TiO_2 plasmon-enhanced HER.

For instance, Zhan et al.[68] proposed a three-dimensional Au embedded in TiO_2 electrode to perform the plasmon-enhanced HER. The system with the best performance was composed of two Au layers embedded in TiO_2. The structure showed an enhanced absorption band in the visible range of the spectrum, centered at 625 nm. The authors addressed this band to a synergic effect of the dielectric interaction of the NP and the semiconductor[68].

The 3D Au-in-TiO_2 structure showed a photocurrent of 1.8 μA/cm^2 at 0.2 $V_{Ag/AgCl}$ (Figure 3A,B), which is five times higher than the one observed for Au-on-TiO_2. Although a plasmonic enhancement was observed, it can not be explained by a direct charge transfer of electrons and holes, as the TiO_2 layers hinder this effect. In this way, simulations were performed and showed an intense electromagnetic field enhancement in the 3D nanostructure, which could explain the observed activity. A strong localized electromagnetic field is formed in the vicinity of Au-TiO_2, inducing the formation of electron-hole pairs. Those pairs are trapped in the embedded structure, guarating an improved charge separation. Finally, the generated electrons are injected in the platinum counter electrode and generate hydrogen, whereas the holes will be collected by the hole scavenger[68]. The mechanism is summarized in Figure 3C.

TiO_2 was also combined with other metals such as Cu[69], Pd[70], and Ag[71,72], making possible to harvest light in the visible and near-infrared range of the spectrum, and using photothermal energy from the NPs to increase the TiO_2 catalytic capability.

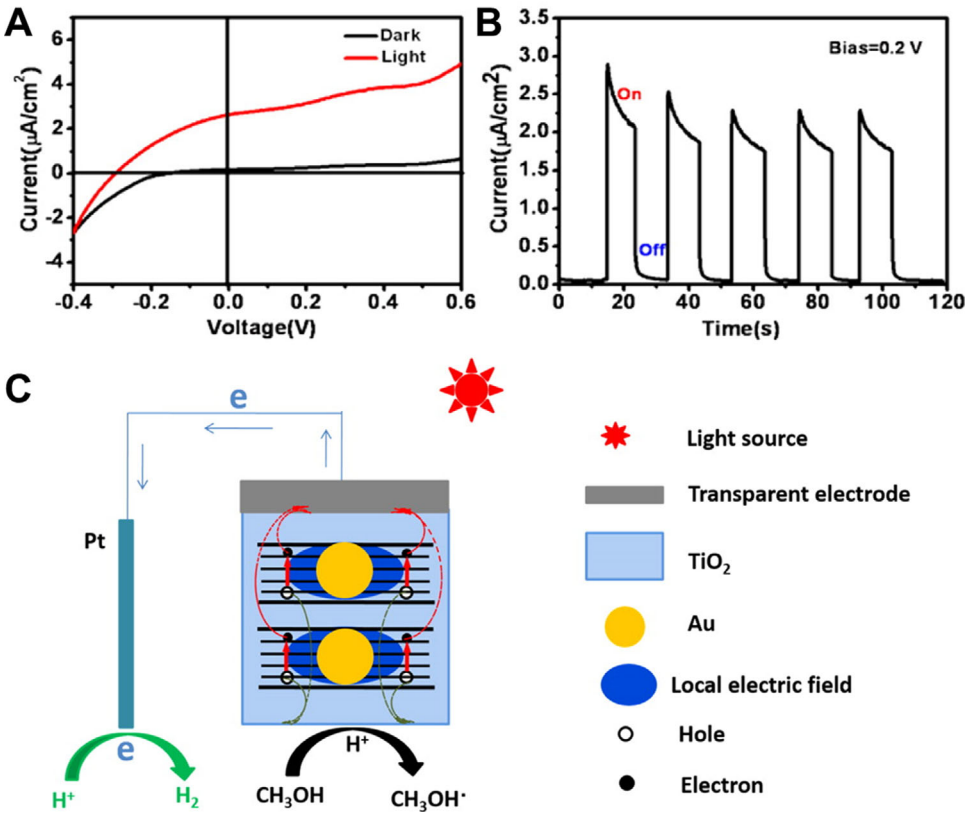

FIGURE 3 **(A)** Polarization curves of under dark and light conditions (Xe lamp) and **(B)** on-off current−time transients at a bias of 0.2 $V_{Ag/AgCl}$ of 3D Au-embedded TiO_2 electrode. **(C)** Schematic illustration of the proposed plasmon-enhanced mechanism of the 3D Au-embedded TiO_2 electrode (two layers of Au particles embedded in TiO_2 matrix). Adapted with permission from ref. [68]. Copyright 2014 American Chemical Society

2.2 | Oxygen evolution reaction

Hematite (α-Fe_2O_3) is a promising photoanode for water splitting applications due to its intrinsic stability, environmental compatibility, and favorable bandgap energy (~1.9–2.3 eV), granting a theoretical maximum solar to hydrogen efficiency of 15 % and the utilization of around 40% of the incident solar radiation[73–75]. Despite its advantages, there are a few drawbacks for its application, such as the relatively low absorption coefficient of visible light, the short lifetime of generated holes, and diffusion length, granting a high recombination rate and low OER kinetics[76,77]. In recent years, gold nanoparticles have been used in order to improve the performance of Fe_2O_3 photoanodes by increasing the absorption of light and the efficiency in the diffusion of holes and electrons due to LSPR[78–81]. Table 2 resumes some of hematite, and other MOs, structures studied for plasmon-assisted OER with Au NPs.

For OER kinetics involving hematite with Au NPs, parameters like the position of the Au on the material[82], thickness of the hematite film[83], and the direct contact of the oxide with Au nanoparticles[84] can cause a poor, or in some cases, a negative effect on the photocurrent of the electrode. A better understanding of these interactions and the mechanisms of charge separation are of great importance for building up an efficient photoanode.

Thimsen et al.[82] compared the photocurrents of Fe_2O_3 in the form of thin films embedded with Au NPs and platelets with the NPs on the surface. It was observed that the Fe_2O_3 modified with gold on the surface, led to a lower photocurrent. The modification with Au NPs produced a negative effect on the catalyst activity. In the embedded configuration the photocurrent increased very slightly, which was due to the introduction of traps in the interface of Au and Fe_2O_3. It was also observed a red shift in the absorbance of the material in the embedded configuration, which Thomann et al.[85] minimized by coating the AuNPs with a thin silica layer. With this methodology, the absorbance of the plasmonic material was maintained at around 550 nm both on top and the bottom of a Fe_2O_3 film. By removing the direct contact of the oxide with the AuNPs, an increase in the photocurrent enhancement was possible, by avoiding the fast recombination effect of charges in Fe_2O_3.

TABLE 2 Comparative materials for OER

Materials	Light source	Electrolyte	Photoconversion	j (mA cm^{-2})	Ref.
Au-Fe_2O_3	300 W Xe lamp 100 mW/cm^2	1.0 M KOH	-	1.0 @ 1.23 V_{RHE}	[82]
Fe_2O_3/Au/ZnO	AM 1.5 G 100 mW/cm^2	0.5 M NaOH	0.02% @ 0,8 V_{RHE}	0.5 @ 0.5 V_{RHE}	[115]
Au/Fe_2O_3	300 W Xe lamp 100 mW/cm^2	1.0 M KOH	-	1.7 @ 1.23 V_{RHE}	[116]
Si/Fe_2O_3/Au	AM 1.5 G 60 mW/cm^2	1.0 M NaOH	6% @ 0 V_{Pt}	2.60 @ 0 V_{Pt}	[86]
Au/Fe2O3	300 W Xe lamp 100 mW/cm^2	1.0 M KOH	-	2.0 @ 1.23 V_{RHE}	[117]
Ti-Fe_2O_3/Al_2O_3/Au	300 W Xe lamp 100 mW/cm^2	1.0 M NaOH	-	1.5 @ 1.23 V_{RHE}	[90]
Au array/Fe_2O_3	AM 1.5 G 100 mW/cm^2	1.0 M KOH	-	1.07 @ 1.23 V_{RHE}	[88]
Au-MnO_2	532 nm laser 200 mW	1.0 M KOH	-	10.0 @ 1.55 V_{RHE}	[101]
Au/Co_3O_4/TiO_2	300 W Xe lamp 100 mW/cm^2	0.5 M Na_2SO_3	-	0.37 @ 1.16 V_{RHE}	[110]
CoOx/Au/TiO_2	Xe lamp 60 mW/cm^2	0.1 M KOH	0.052%	0.003 @ 1.07 V_{RHE}	[118]
Au/CoOOH	525 nm laser 1.2 W	1.0 M KOH	-	10.0 @ 1.52 V_{RHE}	[119]

Also to address the fast recombination of photogenerated holes and electrons in Fe_2O_3, Wang et al.[86] proposed a silicon/hematite core/shell nanowire array as a basis for decorating the material with Au NPs (Figure 4A). In this study, silicon was used for both increasing the absorbance in the long-wavelength part of sunlight and reducing the charges recombination in Fe_2O_3. The photogenerated electrons were transferred to the valence band of silicon, leaving the holes to participate in OER at the Fe_2O_3/H_2O interface (Figure 4B). With the addition of Au NPs localized both on the surface and embedded in the Fe_2O_3, a higher conductivity was obtained. A photocurrent of 2.60 mA/cmš was achieved at 0 V_{Pt} bias in an aqueous 1.0 mol/L NaOH solution, with an efficiency of solar water splitting of 6.0%. Compared with the control material, the overpotential shifted considerably to the negative direction and the photocurrent increased significantly (Figure 4C,D).

Another promising method to decrease recombination rates in Fe_2O_3 is through the passivation of the oxide's surface states. By doing so, the energy transfer mechanism changes to a plasmon-induced resonant energy transfer (PIRET), in which the Au NPs are separated by an insulating material from the Fe_2O_3. In this case, there is no direct electron transfer from Au to the oxide's surface states, and the charge separation is caused by the increase of the localized electromagnetic field from LSPR generated on the plasmonic metal[87–89]. Xu et al.[90] studied a Ti-Fe_2O_3/Al_2O_3/Au photoanode for OER, in which Al_2O_3 acted as an insulating layer between Fe_2O_3 surface states and AuNPs, making PIRET the main mechanism for the separation of charges. The insulating layer also promoted a relaxed Fermi-level pinning, helping to increase band bending and construct a Schottky barrier between Ti-Fe_2O_3 and Au NPs, increasing charge separation. It was observed that with the insulating layer, the recombination rate dropped and, consequently, the photocurrents obtained (1.5 mA/cmš at 1.23V_{RHE}) were more than two times higher than with Ti-Fe_2O_3/Au material.

Aiming for plasmon-assisted OER using Fe_2O_3, AgNPs were also studied.[91–93] These structures also presented an increase in photocurrent and absorption in the visible spectrum. Despite being an alternative plasmonic metal for the reaction, the results obtained are still lower than those obtained with Au NPs, due mainly to the lower work function of Ag (4.26 eV compared with 5.1 eV of Au). When these materials are excited with light, the hot electrons generated by Ag can be injected into the conduction band of Fe_2O_3, which increases the recombination rate[94]. Methods to overcome this limiting effect of Ag NPs

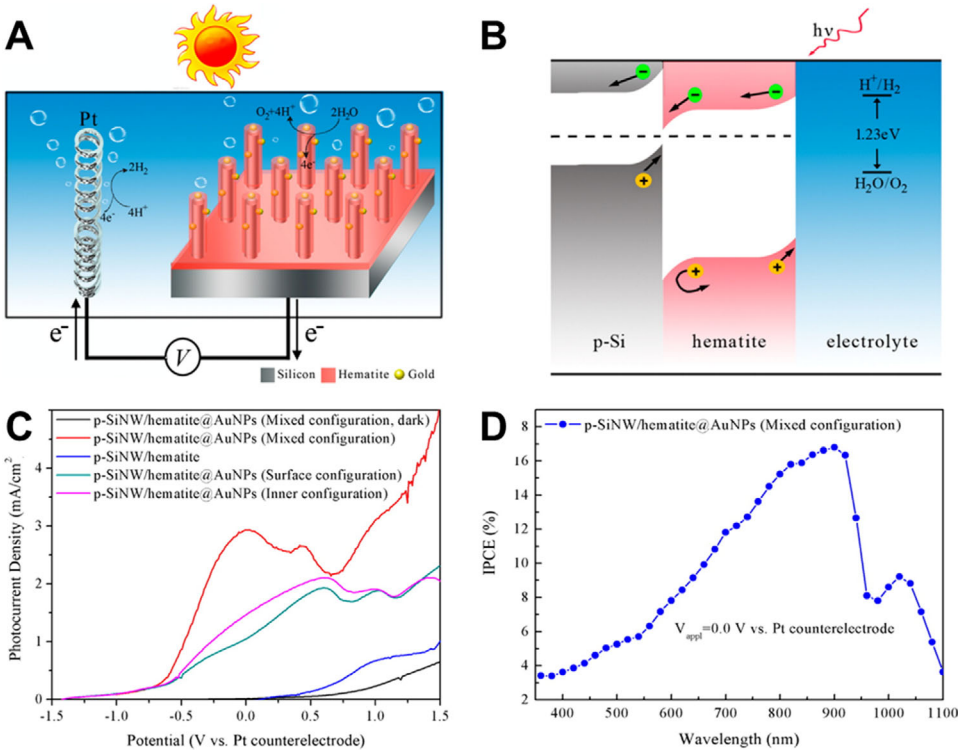

FIGURE 4 **(A)** Schematics of the water-splitting cell containing SiNW/hematite-AuNPs photoanode and **(B)** the approximate band diagram scheme and flow of charges for the material under illumination in contact with electrolyte. **(C)** Photocurrent densities obtained for different configurations of the photoanode under AM 1.5G illumination (60 mW/cm^2) in 1.0 mol/L NaOH, and **(D)** the IPCEs obtained for the mixed configuration under 0 V_{Pt} applied under different wavelengths. Adapted with permission from ref. 86. Copyright 2014 American Chemical Society

focus on the construction of heterostructures using materials with an intermediary work function, achieving higher photocurrents due to a more efficient energy transfer[92,93].

Manganese dioxide is another promising oxide toward the catalysis of OER. Since Morita et al.[95] discovered its remarkable activity for this reaction, MnO_2 has been thoroughly investigated for building up photoanodes towards water splitting in alkaline medium[96,97]. Specifically, thin 2D δ-MnO_2 nanosheets made through defect engineering have been widely studied, as they lead to a great increase in efficiency due to their unique electronic structure[98–100]. Despite the advances made on MnO_2 for OER, the material presents some drawbacks as its low conduction band, limited available active sites, and low conductivity, resulting in lower currents compared with other commonly used MOs[100].

To improve its activity and conductance, Xu et al.[101] proposed a δ-MnO_2 electrode decorated with Au NPs for the LSPR assisted OER on alkaline medium. Under green laser irradiation, the structure achieved an overpotential of 0.32 V, greatly increasing the photocurrent compared to the δ-MnO_2 nanosheets. This increase in performance was explained by the formation of active Mn^+ species by the direct transfer of electrons from MnO_2 to the hot holes generated on gold. The Mn^+ species extract electrons from OH^- in solution more effectively, granting a higher generation of O_2.

Finally, the use of cobalt oxide-based electrodes has been widely studied over the years showing good OER activity in alkaline solutions[102,103]. Among the possible Co oxides, Co_3O_4 is one of the most promising due to the presence of Co^{4+} sites, which is essential for efficient water oxidation[104]. Despite a narrow bandgap (2.1 eV), the conductance band of Co_3O_4 is not negative enough for the photoreduction of water; so, it is usually used with other semiconductors like TiO_2, ZnO, and CuO[105–107] as well as noble metals such as Au and Ag[104,108]. Zhao et al. studied an Au/Co_3O_4/TiO_2 nanorod array as a plasmonic photoanode for water oxidation in 0.5 mol/L Na_2SO_3[110]. The Co_3O_4 and AuNPs generate photoelectrons with visible light illumination, and these electrons are then transferred to the conduction band (CB) of TiO_2 to be used in the reduction of water. Meanwhile, the vacancies generated on Co_3O_4 oxidize water with a higher efficiency, since the removal of electrons by TiO_2 decreases the electron-hole recombination.

3 | CONCLUSION

Recent nanomaterials development and electronic mechanistic insights for photoelectrochemical reaction of noble metal/transition metal oxides hybrid nanoparticles towards water splitting have been briefly described. Considering all the specifics features and the drawbacks for each nanostructure, there are several requirements for the catalysts, such as high chemical and electrochemical stabilities, low cost, facile synthesis, wide absorption band in the visible region of the electromagnetic spectrum, and high charge carriers' lifetime, that are needed to be achieved. The combination of the plasmonic noble metals and aforementioned semiconductors oxides (Sections 2.1 and 2.2) constitute a group of nanostructures that supply most of the essential necessities, nonetheless deeper investigations and developments are demanded.

4 | PERSPECTIVES

In perspective, research in plasmonic electrocatalysis should focus not only on material synthesis, but also on the bottom-neck subject in the field that comprises the mechanism pathway in which the oxidation and reduction reactions take place. Even though there are several hypotheses for the motion of hot carriers, none of them have been definitively indisputable. The separation and identification of the photogenerated charges and the localized increase of temperature, caused by their recombination, contributions to the localized surface plasmon resonance effect is the major issue that still prevents a broadened understanding of the transfer of charge carriers. Therefore, deep electrochemical investigations are needed to be carried out in order to evaluate and comprehend the electronic dynamics. Moreover, beyond the new designs and scientific specificities of the nanomaterials, the focus of the photoelectrochemical studies has encountered some challenges. Mainly, the lack of accurate pattern for reporting plasmonic and electrochemical results deeply masks the real significance and true impact of the outcomes, which cannot be properly compared to each other. Hence, further improvements are expected in the field of plasmon-driven photoelectrochemical reactions to surpass this demand for methodization. Finally, once fulfilled and supplied those requirements and the necessity for standardization of photoelectrochemical results, this type of plasmonic nanomaterials can play a key role in this new solar technology to be implemented on industrial scale and, therefore, constitute a solid branch on the "hydrogen economy."

ACKNOWLEDGMENTS

The authors appreciate the financial support from the São Paulo Research Foundation (FAPESP), grants #2015-26308-7, #2018-16846-0, #2018-22845-6, #2019-15885-4.

DATA AVAILABILITY STATEMENT

Not applicable

ORCID

Susana I. Córdoba de Torresi https://orcid.org/0000-0003-3290-172X

REFERENCES

1. S. Chu, A. Majumdar, *Nature* **2012**, *488*, 294.
2. S. Linic, P. Christopher, D. B. Ingram, *Nat. Mater.* **2011**, *10*, 911.
3. Z. Zheng, W. Xie, B. Huang, Y. Dai, *Chem. – A Eur. J.* **2018**, *24*, 18322.
4. H. Dau, C. Limberg, T. Reier, M. Risch, S. Roggan, P. Strasser, *ChemCatChem* **2010**, *2*, 724.
5. Y. Jiao, Y. Zheng, M. Jaroniec, S. Z. Qiao, *Chem. Soc. Rev.* **2015**, *44*, 2060.
6. M. L. Brongersma, N. J. Halas, P. Nordlander, *Nat. Nanotechnol.* **2015**, *10*, 25.
7. A. B. Dahlin, B. Dielacher, P. Rajendran, K. Sugihara, T. Sannomiya, M. Zenobi-Wong, J. Vörös, *Anal. Bioanal. Chem.* **2012**, *402*, 1773.
8. C. Wang, Y. Shi, D.-R. Yang, X.-H. Xia, *Curr. Opin. Electrochem.* **2018**, *7*, 95.
9. C. Clavero, *Nat. Photonics* **2014**, *8*, 95.
10. T. P. Araujo, J. Quiroz, E. C. M. Barbosa, P. H. C. Camargo, *Curr. Opin. Colloid Interface Sci.* **2019**, *39*, 110.
11. Y. Zhang, S. He, W. Guo, Y. Hu, J. Huang, J. R. Mulcahy, W. D. Wei, *Chem. Rev.* **2018**, *118*, 2927.
12. S. Linic, U. Aslam, C. Boerigter, M. Morabito, *Nat. Mater.* **2015**, *14*, 567.
13. S. Li, P. Miao, Y. Zhang, J. Wu, B. Zhang, Y. Du, X. Han, J. Sun, P. Xu, *Adv. Mater.* **2021**, *33*, 2000086.
14. O. Guselnikova, A. Olshtrem, Y. Kalachyova, I. Panov, P. Postnikov, V. Svorcik, O. Lyutakov, *J. Phys. Chem. C* **2018**, *122*, 26613.
15. Z. Zhang, C. Zhang, H. Zheng, H. Xu, *Acc. Chem. Res.* **2019**, *52*, 2506.
16. C. Wang, X.-G. Nie, Y. Shi, Y. Zhou, J.-J. Xu, X.-H. Xia, H.-Y. Chen, *ACS Nano* **2017**, *11*, 5897.
17. A.-M. Dallaire, S. Patskovsky, A. Vallée-Bélisle, M. Meunier, *Biosens. Bioelectron.* **2015**, *71*, 75.
18. J. Lao, P. Sun, F. Liu, X. Zhang, C. Zhao, W. Mai, T. Guo, G. Xiao, J. Albert, *Light Sci. Appl.* **2018**, *7*, 34.
19. J.-J. Chen, J. C. S. Wu, P. C. Wu, D. P. Tsai, *J. Phys. Chem. C* **2011**, *115*, 210.
20. E. Rodríguez Aguado, J. A. Cecilia, A. Infantes-Molina, A. Talon, L. Storaro, E. Moretti, E. Rodríguez-Castellón, *Dalt. Trans.* **2020**, *49*, 3946.
21. X. Ge, A. Sumboja, D. Wuu, T. An, B. Li, F. W. T. Goh, T. S. A. Hor, Y. Zong, Z. Liu, *ACS Catal.* **2015**, *5*, 4643.
22. C. Acar, I. Dincer, G. F. Naterer, *Int. J. Energy Res.* **2016**, *40*, 1449.
23. C. Lin, Y. Song, L. Cao, S. Chen, *ACS Appl. Mater. Interfaces* **2013**, *5*, 13305.
24. N.-T. Suen, S.-F. Hung, Q. Quan, N. Zhang, Y.-J. Xu, H. M. Chen, *Chem. Soc. Rev.* **2017**, *46*, 337.
25. L. Li, L. Duan, Y. Xu, M. Gorlov, A. Hagfeldt, L. Sun, *Chem. Commun.* **2010**, *46*, 7307.
26. G. Wang, X. Yang, F. Qian, J. Z. Zhang, Y. Li, *Nano Lett.* **2010**, *10*, 1088.

27. Y.-C. Pu, G. Wang, K.-D. Chang, Y. Ling, Y.-K. Lin, B. C. Fitzmorris, C.-M. Liu, X. Lu, Y. Tong, J. Z. Zhang, Y.-J. Hsu, Y. Li, *Nano Lett.* **2013**, *13*, 3817.
28. G. Baffou, R. Quidant, *Chem. Soc. Rev.* **2014**, *43*, 3898.
29. Z. Zhang, L. Zhang, M. N. Hedhili, H. Zhang, P. Wang, *Nano Lett.* **2013**, *13*, 14.
30. G. V Naik, V. M. Shalaev, A. Boltasseva, *Adv. Mater.* **2013**, *25*, 3264.
31. M. Rycenga, C. M. Cobley, J. Zeng, W. Li, C. H. Moran, Q. Zhang, D. Qin, Y. Xia, *Chem. Rev.* **2011**, *111*, 3669.
32. H. Kang, J. T. Buchman, R. S. Rodriguez, H. L. Ring, J. He, K. C. Bantz, C. L. Haynes, *Chem. Rev.* **2019**, *119*, 664.
33. M. Tahir, L. Pan, F. Idrees, X. Zhang, L. Wang, J.-J. Zou, Z. L. Wang, *Nano Energy* **2017**, *37*, 136.
34. J. Wei, M. Zhou, A. Long, Y. Xue, H. Liao, C. Wei, Z. J. Xu, *Nano-Micro Lett.* **2018**, *10*, 75.
35. S. Anantharaj, S. R. Ede, K. Sakthikumar, K. Karthick, S. Mishra, S. Kundu, *ACS Catal.* **2016**, *6*, 8069.
36. A. J. Medford, A. Vojvodic, J. S. Hummelshøj, J. Voss, F. Abild-Pedersen, F. Studt, T. Bligaard, A. Nilsson, J. K. Nørskov, *J. Catal.* **2015**, *328*, 36.
37. Y. Li, Y. Sun, Y. Qin, W. Zhang, L. Wang, M. Luo, H. Yang, S. Guo, *Adv. Energy Mater.* **2020**, *10*, 1903120.
38. I. C. Man, H. Su, F. Calle-Vallejo, H. A. Hansen, J. I. Martínez, N. G. Inoglu, J. Kitchin, T. F. Jaramillo, J. K. Nørskov, *J. Rossmeisl, ChemCatChem* **2011**, *3*, 1159.
39. R. Kavitha, S. G. Kumar, *Mater. Sci. Semicond. Process.* **2019**, *93*, 59.
40. K. Qi, B. Cheng, J. Yu, W. Ho, *J. Alloys Compd.* **2017**, *727*, 792.
41. P. Fageria, S. Gangopadhyay, S. Pande, *RSC Adv.* **2014**, *4*, 24962.
42. S. Kattel, P. J. Ramírez, J. G. Chen, J. A. Rodriguez, P. Liu, *Science (80)* **2017**, *355*, 1296.
43. S. Mubeen, J. Lee, W. Lee, N. Singh, G. D. Stucky, M. Moskovits, *ACS Nano* **2014**, *8*, 6066.
44. Z. Zhang, J. T. Yates, *Chem. Rev.* **2012**, *112*, 5520.
45. N. Güy, M. Özacar, *Int. J. Hydrogen Energy* **2016**, *41*, 20100.
46. X. Zhang, Y. Liu, Z. Kang, *ACS Appl. Mater. Interfaces* **2014**, *6*, 4480.
47. S. W. Kang, P. R. Deshmukh, Y. Sohn, W. G. Shin, *Mater. Today Commun.* **2019**, *21*, 100675.
48. C. Mahala, M. D. Sharma, M. Basu, *ACS Appl. Nano Mater.* **2020**, *3*, 1153.
49. W. Zhang, W. Wang, H. Shi, Y. Liang, J. Fu, M. Zhu, *Sol. Energy Mater. Sol. Cells* **2018**, *180*, 25.
50. Y. Liu, X. Yan, Z. Kang, Y. Li, Y. Shen, Y. Sun, L. Wang, Y. Zhang, *Sci. Rep.* **2016**, *6*, 29907.
51. Y.-H. Chiu, K.-D. Chang, Y.-J. Hsu, *J. Mater. Chem. A* **2018**, *6*, 4286.
52. M. Wu, W.-J. Chen, Y.-H. Shen, F.-Z. Huang, C.-H. Li, S.-K. Li, *ACS Appl. Mater. Interfaces* **2014**, *6*, 15052.
53. H. M. Chen, C. K. Chen, M. L. Tseng, P. C. Wu, C. M. Chang, L.-C. Cheng, H. W. Huang, T. S. Chan, D.-W. Huang, R.-S. Liu, D. P. Tsai, *Small* **2013**, *9*, 2926.
54. A. Sreedhar, I. Neelakanta Reddy, Q. T. H. Ta, G. Namgung, J.-S. Noh, *J. Electroanal. Chem.* **2019**, *832*, 426.
55. Y. Wei, L. Ke, J. Kong, H. Liu, Z. Jiao, X. Lu, H. Du, X. W. Sun, *Nanotechnology* **2012**, *23*, 235401.
56. J. Zhang, W. Wang, X. Liu, *Mater. Lett.* **2013**, *110*, 204.
57. H. Liu, Y. Hu, Z. Zhang, X. Liu, H. Jia, B. Xu, *Appl. Surf. Sci.* **2015**, *355*, 644.
58. A. Fujishima, K. Honda, *Nature* **1972**, *238*, 37.
59. X. Yang, X. Wu, J. Li, Y. Liu, *RSC Adv.* **2019**, *9*, 29097.
60. A. S. Hainer, J. S. Hodgins, V. Sandre, M. Vallieres, A. E. Lanterna, J. C. Scaiano, *ACS Energy Lett.* **2018**, *3*, 542.
61. J. Abed, N. S. Rajput, A. El Moutaouakil, M. Jouiad, *Nanomaterials* **2020**, *10*, 2260.
62. H. Wang, T. You, W. Shi, J. Li, L. Guo, *J. Phys. Chem. C* **2012**, *116*, 6490.
63. J. Zhang, X. Jin, P. I. Morales-Guzman, X. Yu, H. Liu, H. Zhang, L. Razzari, J. P. Claverie, *ACS Nano* **2016**, *10*, 4496.
64. S. Choi, Y. S. Nam, *ACS Appl. Energy Mater.* **2018**, *1*, acsaem.7b00262.
65. M.-I. Mendoza-Diaz, J. Cure, M. D. Rouhani, K. Tan, S.-G. Patnaik, D. Pech, M. Quevedo-Lopez, T. Hungria, C. Rossi, A. Estève, *J. Phys. Chem. C* **2020**, *124*, 25421.
66. Y. Wang, J. Yu, W. Xiao, Q. Li, *J. Mater. Chem. A* **2014**, *2*, 3847.
67. W. Jiang, S. Bai, L. Wang, X. Wang, L. Yang, Y. Li, D. Liu, X. Wang, Z. Li, J. Jiang, Y. Xiong, *Small* **2016**, *12*, 1640.
68. Z. Zhan, J. An, H. Zhang, R. V. Hansen, L. Zheng, *ACS Appl. Mater. Interfaces* **2014**, *6*, 1139.
69. R. Song, M. Liu, B. Luo, J. Geng, D. Jing, *AIChE J.* **2020**, *66*, 1–10.
70. Y. Zhu, Z. Xu, W. Jiang, W. Yin, S. Zhong, P. Gong, R. Qiao, Z. Li, S. Bai, *RSC Adv.* **2016**, *6*, 56800.
71. L. Sang, H. Ge, B. Sun, *Int. J. Hydrogen Energy* **2019**, *44*, 15787.
72. R. A. Rather, S. Singh, B. Pal, *Sol. Energy Mater. Sol. Cells* **2017**, *160*, 463.
73. M. Mishra, D.-M. Chun, *Appl. Catal. A Gen.* **2015**, *498*, 126.
74. J. E. Turner, M. Hendewerk, J. Parmeter, D. Neiman, G. A. Somorjai, *J. Electrochem. Soc.* **1984**, *131*, 1777.
75. B. M. Hunter, H. B. Gray, A. M. Müller, *Chem. Rev.* **2016**, *116*, 14120.
76. J. Deng, X. Lv, J. Zhong, *J. Phys. Chem. C* **2018**, *122*, 29268.
77. K. G. Upul Wijayantha, S. Saremi-Yarahmadi, L. M. Peter, *Phys. Chem. Chem. Phys.* **2011**, *13*, 5264.
78. Y. Fu, C.-L. Dong, W. Zhou, Y.-R. Lu, Y.-C. Huang, Y. Liu, P. Guo, L. Zhao, W.-C. Chou, S. Shen, *Appl. Catal. B Environ.* **2020**, *260*, 118206.
79. W. Xiong, Q. Zhao, X. Li, L. Wang, *Part. Part. Syst. Charact.* **2016**, *33*, 602.
80. L. Wang, H. Hu, N. T. Nguyen, Y. Zhang, P. Schmuki, Y. Bi, *Nano Energy* **2017**, *35*, 171.
81. E. Thimsen, F. Le Formal, M. Grätzel, S. C. Warren, *Nano Lett.* **2011**, *11*, 35.
82. L. Wang, X. Zhou, N. T. Nguyen, P. Schmuki, *ChemSusChem* **2015**, *8*, 618.
83. P. S. Archana, N. Pachauri, Z. Shan, S. Pan, A. Gupta, *J. Phys. Chem. C* **2015**, *119*, 15506.
84. J. Zheng, H. Zhou, Y. Zou, R. Wang, Y. Lyu, S. P. Jiang, S. Wang, *Energy Environ. Sci.* **2019**, *12*, 2345.
85. I. Thomann, B. A. Pinaud, Z. Chen, B. M. Clemens, T. F. Jaramillo, M. L. Brongersma, *Nano Lett.* **2011**, *11*, 3440.
86. X. Wang, K.-Q. Peng, Y. Hu, F.-Q. Zhang, B. Hu, L. Li, M. Wang, X.-M. Meng, S.-T. Lee, *Nano Lett.* **2014**, *14*, 18.
87. J. Li, S. K. Cushing, F. Meng, T. R. Senty, A. D. Bristow, N. Wu, *Nat. Photonics* **2015**, *9*, 601.
88. Y. M. Choi, B. W. Lee, M. S. Jung, H. S. Han, S. H. Kim, K. Chen, D. H. Kim, T. F. Heinz, S. Fan, J. Lee, G.-R. Yi, J. K. Kim, J. H. Park, *Adv. Energy Mater.* **2020**, *10*, 2000570.
89. Y. Liu, Z. Xu, M. Yin, H. Fan, W. Cheng, L. Lu, Y. Song, J. Ma, X. Zhu, *Nanoscale Res. Lett.* **2015**, *10*, 374.

90. Z. Xu, Z. Fan, Z. Shi, M. Li, J. Feng, L. Pei, C. Zhou, J. Zhou, L. Yang, W. Li, G. Xu, S. Yan, Z. Zou, *ChemSusChem* **2018**, *11*, 237.
91. I. N. Reddy, C. V. Reddy, A. Sreedhar, M. Cho, D. Kim, J. Shim, *J. Electroanal. Chem.* **2019**, *842*, 146.
92. L. Yu, Y. Zhang, J. He, H. Zhu, X. Zhou, M. Li, Q. Yang, F. Xu, *J. Alloys Compd.* **2018**, *753*, 601.
93. I. Khan, A. Qurashi, *ACS Sustain. Chem. Eng.* **2018**, *6*, 11235.
94. S. Zhang, F. Ren, W. Wu, J. Zhou, L. Sun, X. Xiao, C. Jiang, *J. Colloid Interface Sci.* **2014**, *427*, 29.
95. M. Morita, C. Iwakura, H. Tamura, *Electrochim. Acta* **1977**, *22*, 325.
96. X. Cheng, G. Dong, Y. Zhang, C. Feng, Y. Bi, *Appl. Catal. B Environ.* **2020**, *267*, 118723.
97. B. A. Pinaud, Z. Chen, D. N. Abram, T. F. Jaramillo, *J. Phys. Chem. C* **2011**, *115*, 11830.
98. Y. Zhao, C. Chang, F. Teng, Y. Zhao, G. Chen, R. Shi, G. I. N. Waterhouse, W. Huang, T. Zhang, *Adv. Energy Mater.* **2017**, *7*, 1700005.
99. C. Wang, F. Wang, S.-Y. Qiu, J. Gao, L.-L. Gu, K.-X. Wang, P.-J. Zuo, K.-N. Sun, X.-D. Zhu, *Int. J. Hydrogen Energy* **2021**, *46*, 10356.
100. J. Lu, H. Wang, Y. Sun, X. Wang, X. Song, R. Wang, *Chem. Eng. J.* **2020**, 127894.
101. J. Xu, P. Gu, D. J. S. Birch, Y. Chen, *Adv. Funct. Mater.* **2018**, *28*, 1801573.
102. K. Xie, J. Masa, E. Madej, F. Yang, P. Weide, W. Dong, M. Muhler, W. Schuhmann, W. Xia, *ChemCatChem* **2015**, *7*, 3027.
103. A. J. Esswein, M. J. McMurdo, P. N. Ross, A. T. Bell, T. D. Tilley, *J. Phys. Chem. C* **2009**, *113*, 15068.
104. B. S. Yeo, A. T. Bell, *J. Am. Chem. Soc.* **2011**, *133*, 5587.
105. G. Dai, S. Liu, Y. Liang, T. Luo, *Appl. Surf. Sci.* **2013**, *264*, 157.
106. H. Wu, S. Li, X. Lu, C. Y. Toe, H. Y. Chung, Y. Tang, X. Lu, R. Amal, L. Li, Y. H. Ng, *Chempluschem* **2018**, *83*, 934.
107. G. Hu, C.-X. Hu, Z.-Y. Zhu, L. Zhang, Q. Wang, H.-L. Zhang, *ACS Sustain. Chem. Eng.* **2018**, *6*, 8801.
108. Y. Zhang, J. Nie, Q. Wang, X. Zhang, Q. Wang, Y. Cong, *Appl. Surf. Sci.* **2018**, *427*, 1009.
109. X. Zhao, W. Wang, Y. Liang, L. Yao, J. Fu, H. Shi, C. Tao, *Int. J. Hydrogen Energy* **2019**, *44*, 14561.
110. R. Reichert, Z. Jusys, R. J. Behm, *J. Phys. Chem. C* **2015**, *119*, 24750.
111. Y. Sun, B. Xu, Q. Shen, L. Hang, D. Men, T. Zhang, H. Li, C. Li, Y. Li, *ACS Appl. Mater. Interfaces* **2017**, *9*, 31897.
112. T. Wang, R. Lv, P. Zhang, C. Li, J. Gong, *Nanoscale* **2015**, *7*, 77.
113. A. Sreedhar, I. N. Reddy, J. H. Kwon, J. Yi, Y. Sohn, J. S. Gwag, J.-S. Noh, *Ceram. Int.* **2018**, *44*, 18978.
114. T. Liu, W. Chen, T. Huang, G. Duan, X. Yang, X. Liu, *J. Mater. Sci.* **2016**, *51*, 6987.
115. R. Kant, S. Pathak, V. Dutta, *Sol. Energy Mater. Sol. Cells* **2018**, *178*, 38.
116. F. Lei, H. Liu, J. Yu, Z. Tang, J. Xie, P. Hao, G. Cui, B. Tang, *Phys. Chem. Chem. Phys.* **2019**, *21*, 1478.
117. L. Wang, T. Nakajima, Y. Zhang, *J. Mater. Chem. A* **2019**, *7*, 5258.
118. M. Okazaki, Y. Suganami, N. Hirayama, H. Nakata, T. Oshikiri, T. Yokoi, H. Misawa, K. Maeda, *ACS Appl. Energy Mater.* **2020**, *3*, 5142.
119. S. Feng, L. Yang, Z. Zhang, Q. Li, D. Xu, *ACS Appl. Energy Mater.* **2020**, *3*, 943.

AUTHOR BIOGRAPHIES

Maria Paula de Souza Rodrigues obtained a BS degree from Universidade Federal Fluminense (2016). She is currently a PhD candidate in chemistry at Prof. Dr. Susana I. Córdoba de Torresi team. Her research focuses on the synthesis and electrochemical application of plasmonic nanostructures.

Vítor Mendes Miguel obtained a BS in chemistry from the Universidade Federal do Rio de Janeiro in 2019. He is currently a Master's candidate in chemistry at Universidade de São Paulo. His current research focuses on the synthesis and electrochemical applications of plasmonic nanostructures.

Lucas Dias Germano obtained a BS degree in chemistry with technological attributions from Mackenzie Presbyterian University (2018). He is currently a PhD candidate in chemistry at Prof. Dr. Susana I. Córdoba de Torresi team. His research interests are focused on development and electrochemical application of plasmonic nanomaterials.

Susana I. Cordoba de Torresi graduated in physical chemistry at Universidad Nacional de Córdoba, Argentina, where she also concluded PhD in chemistry with emphasis in electrochemistry. She was a posdoc fellow at Université de Paris VI, France, Physics Institute of UNICAMP, Brazil and Chemistry Department of UFSCar, Brazil. Presently, she is a full professor of the Institute of Chemistry, Universidade de São Paulo since 1996. She was vice-president of the International Society of Electrochemistry and has received several national and international awards and honors such as the Tajima Prize (International Society of Electrochemistry), National Order of Scientific Merit, she is a member of the Brazilian Academy of Sciences and of the Academy of Sciences of the State of São Paulo. Her interests are in the field of electrocatalysis, nanotechnology, and tailoring of new materials.

How to cite this article: M. P. S. Rodrigues, V. M. Miguel, L. D. Germano, S. I. Córdoba de Torresi. *Electrochem Sci Adv*. **2022**, *2,* e2100079. https://doi.org/10.1002/elsa.202100079